

1 **Selective amide bond formation in redox-active coacervate protocells**

2 Jiahua Wang,^[a] Manzar Abbas,^[a] Junyou Wang^{*[b]} and Evan Spruijt^{*[a]}

3
4 ^[a]Radboud University, Institute for Molecules and Materials, Heyendaalseweg 135, 6525 AJ Nijmegen, the Netherlands

5 ^[b] State Key Laboratory of Chemical Engineering and Shanghai Key Laboratory of Multiphase Materials Chemical
6 Engineering, East China University of Science and Technology, Shanghai 200237, China

7 *Email: e.spruijt@science.ru.nl, junyouwang@ecust.edu.cn

8

9 **Abstract**

10 Membraneless compartments, like complex coacervates droplets, are promising protocell models
11 because of their ability to sequester a wide range of guest molecules and their catalytic properties.
12 However, it remains unclear how the building blocks of life, including peptides, could be
13 synthesized from primitive precursor molecules inside such protocells. Here, we develop a new
14 protocell model formed by phase separation of prebiotically relevant small redox-active
15 ferricyanide ($\text{Fe}(\text{CN})_6^{3-}$)/ferrocyanide ($\text{Fe}(\text{CN})_6^{4-}$) molecules and a cationic peptide. The assembly
16 of these coacervate protocells can be regulated by redox chemistry and they act as oxidizing hubs
17 for sequestered metabolites, such as NAD(P)H, and fiber precursors. Interestingly, we show that
18 the oxidizing potential of ferricyanide inside coacervates can be harnessed to drive the selective
19 formation of amide bonds between prebiotically relevant amino thioacids and amino acids or
20 peptides. We demonstrate that aminoacylation is enhanced in $\text{Fe}(\text{CN})_6^{3-}$ /peptide coacervate
21 dispersions compared to the surrounding dilute phase, and selective for amino acids that interact
22 less strongly with the coacervates. We finally use this amide bond formation to create self-

23 reinforcing coacervates by reacting hydrophobic amino thioacids to amines on the protocell
24 scaffold and show that this significantly enhances their salt resistance. These results provide an
25 important step towards the prebiotically relevant integration of redox chemistry in cell-like
26 compartments.

27

28

29 **Introduction**

30 Amide bond formation is an essential chemical reaction in all forms of life that is catalyzed by
31 highly evolved biomolecular machinery. However, before ribosomes and specialized enzymes
32 became capable of protein synthesis,^{1,2} alternative, simple prebiotic routes to create peptide bonds
33 in a spatiotemporally controlled way likely existed. Protocellular compartments provide a
34 promising platform to localize chemical reactions relevant to life.³⁻⁵ What the nature of such
35 protocellular compartments capable of peptide synthesis could be, remains unknown. As plausible
36 precursors to peptides, α -aminothioacids (AA-SH)⁶ and acetylated aminothioacids (Ac-AA-SH)⁷
37 have been shown to be formed in aqueous conditions at near-neutral pH. They are considered
38 interesting alternatives to biological thioesters for prebiotic peptide ligation, and can be ligated into
39 peptide with the aid of an oxidizing catalyst, such as ferricyanide.⁷⁻¹⁰ However, high concentrations
40 of reactants and catalysts are typically required for these oxidative peptide ligations, which may
41 not have been easy to reach. Recent work has demonstrated that some micro-compartments and
42 protocell systems could compartmentalize (bio)chemical reactions, and act as catalytic
43 microreactors or reaction localization centers with potential for prebiotic peptide ligation.¹¹⁻¹⁶

44 In particular, membraneless compartments based on complex coacervates have been
45 considered as versatile protocell models in the origins of life research.^{5,16-19} Coacervate droplets

46 are formed spontaneously by liquid-liquid phase separation, resulting in a polymer- or peptide-rich,
47 cell-sized dense coacervate phase, and a coexisting dilute phase. These membraneless droplets can
48 easily take up and concentrate guest molecules from their surroundings due to charge
49 complementarity or hydrophobicity.^{16,20,21} The ability to up-concentrate and exchange guests make
50 the coacervate droplets capable of supporting biochemical reactions, and sometimes enhancing the
51 activity of catalysts, such as ribozymes,^{12,13} or enzymes in cascade reactions,^{15,22} thereby increasing
52 the overall rate. Recent work has demonstrated that coacervate droplets can be active,^{18,23} and that
53 their formation and dissolution can be regulated by environmental changes, such as pH,^{24,25}
54 temperature,^{26,27} light,²⁸ enzymatic reactions,^{23,29-31} or fuel-driven chemical reaction cycles.¹⁸

55 To date, research on coacervates as reaction localization centers has mostly focused on
56 enzymatic reactions, or reactions involving complex RNAzymes (ribozymes). However, the
57 fundamental biochemical reactions that lead to the formation of peptides, which themselves are
58 often the building blocks of coacervates, have not been studied. For coacervates to be a plausible
59 protocell model, they must be able to support a prebiotically relevant ligation reaction of peptides,
60 and ultimately, link this reaction to the construction of new coacervates. Here, we show that
61 ferricyanide-containing coacervates can potentially fulfill this role. These coacervates can be used
62 to oxidize not only a variety of common metabolites, but also amino thioacids, which can
63 subsequently be aminoacylated yielding a product with a new amide bond.

64 Coacervates with ferrocyanide, the reduced form of ferricyanide, as multivalent anion have
65 already been reported by Bungenberg-de Jong and Kruyt in 1929.³² They used gelatin at low pH
66 as a long polycation and observed small punctated droplets upon mixing with potassium
67 ferrocyanide. However, the redox potential of the iron centers inside these coacervates remains
68 unclear. More recently, it was shown that coacervates can be formed from much smaller cationic
69 oligopeptides, such as oligolysine and oligoarginine with as little as five amino acids, complexed

70 with either small tri- or tetravalent anions, like ADP and ATP.¹⁹ We therefore hypothesized that it
71 should be possible to make coacervates of the redox couple ferri- and ferrocyanide with a cationic
72 polypeptide in such a way that ferrocyanide, the reduced state with a 4⁻ charge, would form stable
73 droplets, but ferricyanide, the oxidized state with a 3⁻ charge, would not. This would enable the
74 selective compartmentalization of guest molecules only under certain redox potential in the
75 environment. In addition, from an origins of life perspective, the environment on early Earth was
76 likely depleted of oxygen, a strong oxidizing agent that is widely used in living systems, for a
77 considerable period. Alternative oxidizing agents, such as ferricyanide ($\text{Fe}(\text{CN})_6^{3-}$), could have has
78 been essential in the prebiotic activation of building blocks for peptide ligation,^{7,9,33,34} and oxidation
79 of metabolites.³⁵ By condensing the ferricyanide with an oppositely charged peptide at low ionic
80 strength, it may be possible to localize these reactions in a droplet compartment and enrich the
81 coacervate with the products of ferricyanide-catalyzed oxidation reactions.

82 Here, we show that both ferricyanide and ferrocyanide ions can be condensed into coacervate
83 droplets with short cationic polypeptides depending on the ionic strength. These droplets are
84 responsive and can be regulated by redox chemistry. They act as prebiotic oxidizing hubs for
85 metabolites and common electron donors, such as NADH, NADPH and GSH, thus taking the role
86 of oxygen as terminal electron acceptor. Besides small metabolites, aromatic thiols such as benzoyl
87 cysteine can be oxidized inside ferricyanide-based coacervates, leading to their assembly into
88 stacked filaments, which further bundle into rigid fibers that resemble a cytoskeletal network inside
89 and around the protocells. Moreover, we show that the oxidizing potential of ferricyanide-based
90 coacervates can be harnessed to drive the formation of peptide bonds between amino acid and
91 amino thioacids which are considered as potential prebiotic precursors of amino acids. We
92 demonstrate that amino thioacid ligation is enhanced in $\text{Fe}(\text{CN})_6^{3-}$ /peptide coacervate dispersions
93 compared to the surrounding dilute phase due to the local high ferricyanide concentration. The

94 coacervate environment imposes a selection pressure that results in kinetic pathway selection and
95 a strong, preferential incorporation of certain amino acids. When amino acids or short peptides are
96 used as client substrates, the reaction products can leave the coacervate droplets again, but they can
97 also be anchored to the coacervate compartments by using peptides containing amine groups as
98 coacervating scaffolds. We show that this strategy can be used to create self-reinforcing
99 coacervates, in which hydrophobic amino acid residues are ligated to the coacervate building
100 blocks and enhance their stability. In short, our results show that prebiotically relevant ferricyanide-
101 based coacervate protocells are versatile oxidizing hubs that exist in aqueous solution, in which
102 metabolites can be converted, fibrous networks assembled and peptides synthesized.

103

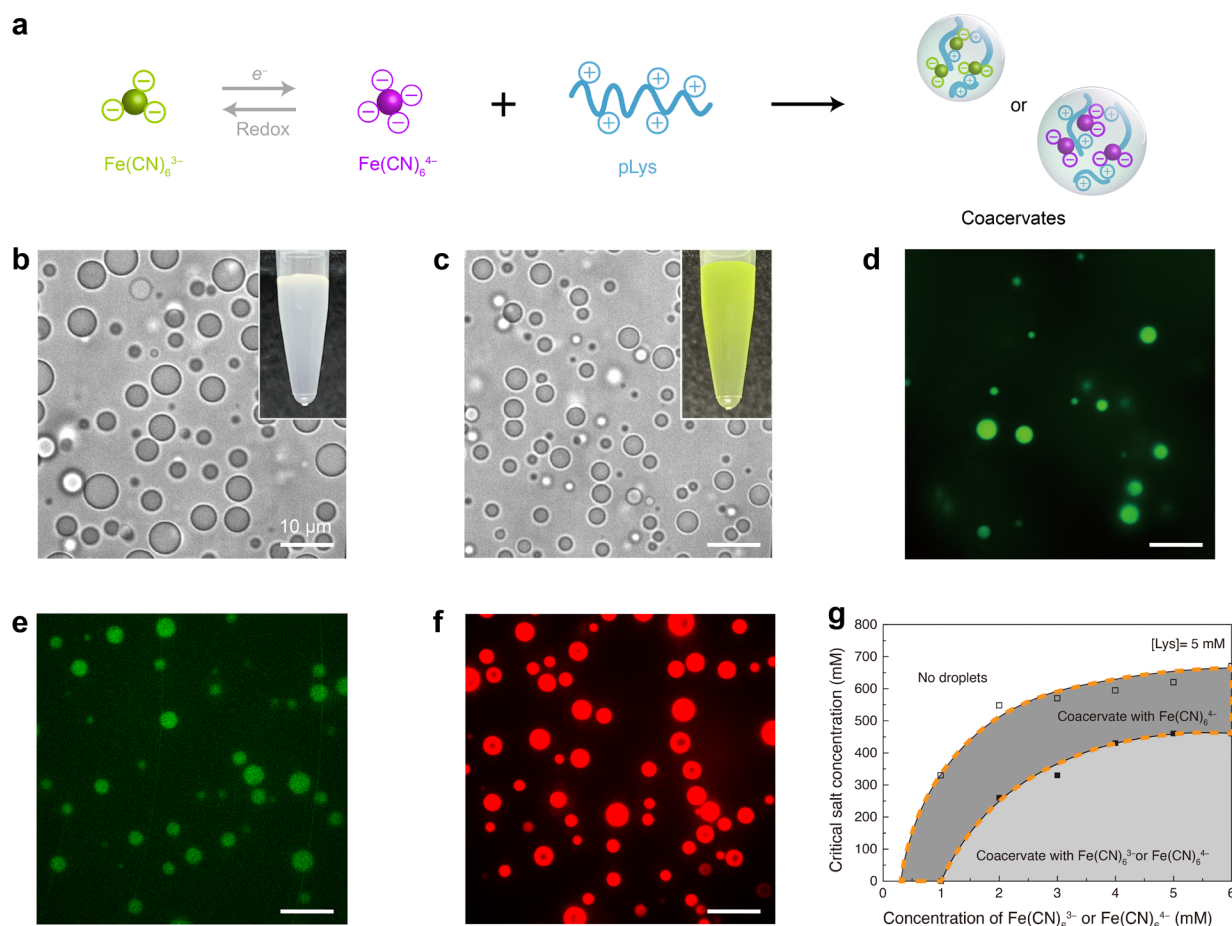
104 **Results and discussion**

105 **Coacervation of ferricyanide/ferrocyanide and polypeptides**

106 Small, multivalent ions can be condensed into liquid coacervate droplets by complexation with an
107 oppositely charged peptide or polymer.⁵ We sought to use this principle to create coacervate
108 protocells that can concentrate a prebiotically relevant redox catalyst to enable localized peptide
109 synthesis. Ferricyanide is a trivalent anion and its reduced form, the tetravalent ferrocyanide, has
110 been shown to be able to form coacervates with gelatin at low pH.³² We used cationic peptides to
111 induce phase separation of ferri- and ferrocyanide. Spherical complex (heterotypic) coacervate
112 droplets were readily formed as a turbid dispersion via spontaneous liquid-liquid phase separation
113 associated with the charge neutralization of a range of peptides ((Lys)₁₀, (Lys)₂₀, (Lys(Me)₃)₂₀,
114 (Lys)₃₀, (Lys(Me)₃)₃₀, poly-L-lysine (pLys) and (Arg)₁₀) in the presence of ferrocyanide or
115 ferricyanide (Fig. 1a, Supplementary Fig. 4). (Arg)₁₀ formed coacervates with both ferrocyanide
116 and ferricyanide, while (Lys)₁₀/(Lys)₂₀ only formed coacervates with tetravalent ferrocyanide in

117 salt-free solution. The difference between (Lys)₁₀ and (Arg)₁₀ can be explained by the higher p*K*_a
 118 of the basic residue in arginine compared to lysine, which may generate more stable ionic
 119 interactions at a given chain length.³⁶ Increasing the length of polylysine to (Lys)₃₀ resulted in the
 120 formation of coacervates with trivalent ferricyanide as well (Supplementary Fig. 4c), in agreement
 121 with previous studies involving nucleotides.^{19,27}

122



123
 124 **Figure 1.** (a) Schematic illustration of associative liquid-liquid phase separation of Fe(CN)₆³⁻/Fe(CN)₆⁴⁻ and pLys to
 125 produce coacervate droplets. (b) Optical microscope images of Fe(CN)₆⁴⁻/pLys droplets prepared at 1 mM Fe(CN)₆⁴⁻
 126 and 5 mM pLys (monomer basis), and (c) at 2 mM Fe(CN)₆³⁻ and 5 mM pLys (monomer basis). Insets show
 127 photographs of the corresponding turbid suspensions. (d-f) Fluorescence microscopy images of Fe(CN)₆⁴⁻/pLys
 128 droplets with various client molecules: (d) pyranine, (e) NADPH, (f) poly-rU₁₅ (scale bars indicate 10 μm). (g)
 129 Critical salt concentration of Fe(CN)₆³⁻ and Fe(CN)₆⁴⁻ coacervates with a fixed concentration of 5 mM pLys, determined from
 130 turbidity titrations.

131 The obtained coacervates with a diameter of about 2 to 3 μm were observed in a PLL-g-PEG
132 functionalized microchamber (Figure 1b-c). These microdroplets exhibited liquid-like properties:
133 they wetted the bottom glass surface and sedimenting coacervates coalesced with coacervates
134 already present at the bottom of the microchambers to form bigger droplets. The droplets
135 sequestered negatively charged client solutes, including pyranine, NAD(P)H, and ribonucleic acids
136 (Figure 1d-f, Supplementary Fig. 4). Determination of the partitioning of ferricyanide and
137 ferrocyanide by Uv-vis spectroscopy (see Methods) showed that both these multivalent scaffolding
138 anions were highly concentrated in the coacervate droplets: the internal concentration in coacervate
139 droplets was 100 times higher than the surrounding dilute aqueous phase. For example, for samples
140 prepared from 2 mM ferricyanide and pLys (5mM lysine monomers) solutions, we found an
141 internal ferricyanide concentration of ~ 30 mM, compared to ~ 0.3 mM in the surrounding aqueous
142 phase. (Supplementary Fig. 5). Surprisingly, the concentration ratio for ferri- and ferrocyanide was
143 the same, despite their different valency. We attribute this to the formation of a tighter complex
144 between ferricyanide and polycations, which results in a more hydrophobic coacervate,²⁷ an effect
145 that has previously been observed with ferricyanide in polyelectrolyte brushes.³⁷ A similar 100x
146 concentration was previously found for a negatively charged bis-carboxylic acid ligand, which can
147 exist in a tetravalent (4-) ring configuration, in coacervates with cationic polymers.³⁸ These initial
148 observations suggest that the spontaneous assembly of peptides and ferricyanide or ferrocyanide
149 could be developed as potential prebiotic membraneless compartments.

150 Typically, coacervates formed by charge-charge interaction are sensitive to the ionic strength
151 and they exhibit a critical salt concentration (CSC) above which phase separation does not take
152 place. Since ferricyanide and ferrocyanide have a different net charge, their CSC is likely different,
153 even though the previously discussed hydration differences may decrease that effect. A difference
154 in CSC would allow for selective compartmentalization controlled by redox chemistry. To

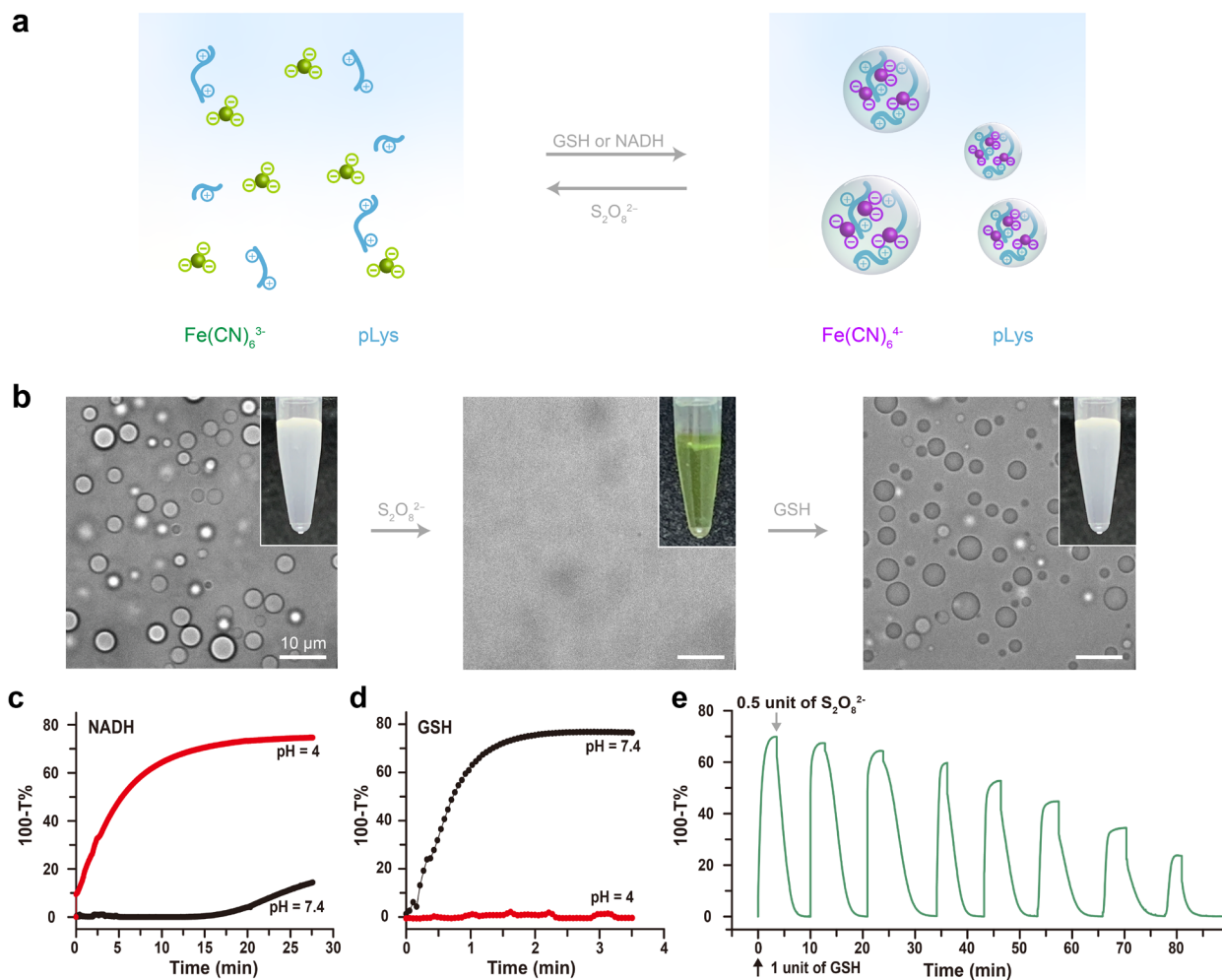
155 determine the conditions under which the redox couple ferri- and ferrocyanide could give rise to
156 reversible coacervate formation and dissolution, we evaluated the salt resistance of $\text{Fe}(\text{CN})_6^{4-}$ and
157 $\text{Fe}(\text{CN})_6^{3-}$ -based coacervates. As a model peptide, we focused on pLys ($M_w = 15\text{-}30$ kDa).
158 Supplementary Fig. 6 shows turbidity-based titration curves of pLys (5 mM monomer units), as a
159 function of $\text{Fe}(\text{CN})_6^{4-}$ or $\text{Fe}(\text{CN})_6^{3-}$, and as a function of salt concentration. From plots of the
160 turbidity we determined the critical salt concentration (CSC), the point at which coacervate droplets
161 completely disappear. Figure 1g shows the resulting phase diagram of both $\text{Fe}(\text{CN})_6^{4-}$ and
162 $\text{Fe}(\text{CN})_6^{3-}$ coacervates. As expected, $\text{Fe}(\text{CN})_6^{4-}$ -based coacervates have a higher salt resistance,
163 expressed by their CSC, compared to $\text{Fe}(\text{CN})_6^{3-}$ -based coacervates. Our results are in good
164 agreement with previous studies with nucleotide/pLys-based coacervates, where the ATP/pLys
165 droplets have a higher CSC than ADP/pLys droplets, in line with their valency.^{19,30}

166

167 **Redox chemistry of ferri/ferrocyanide in coacervates**

168 We next exploited the redox activity of the droplets in the critical salt concentration window
169 highlighted in Fig. 1g. To illustrate the feasibility of the redox cycling proposed in Fig. 2a to induce
170 phase separation and droplet dissolution, we prepared mixtures of $\text{Fe}(\text{CN})_6^{4-}$ with pLys and
171 $\text{Fe}(\text{CN})_6^{3-}$ with pLys under identical conditions within the highlighted region of Fig. 1g between
172 the two binodal lines. The original $\text{Fe}(\text{CN})_6^{4-}$ -containing mixtures and $\text{Fe}(\text{CN})_6^{3-}$ -containing
173 mixtures are white turbid and yellowish transparent, respectively. When observed under the
174 microscope, the $\text{Fe}(\text{CN})_6^{4-}$ -containing mixtures had clearly condensed into droplets, while the
175 $\text{Fe}(\text{CN})_6^{3-}$ -containing mixtures remained a homogeneous solution. Upon oxidation of the $\text{Fe}(\text{CN})_6^{4-}$
176 -coacervates by $\text{S}_2\text{O}_8^{2-}$, the originally white turbid solution turned yellowish transparent, and no
177 droplets could be observed under the microscope (Fig. 2b). Conversely, after reduction of the
178 $\text{Fe}(\text{CN})_6^{3-}$ -containing mixtures with GSH or NADH (Fig. 2b-d), the original, light-yellow

179 transparent $\text{Fe}(\text{CN})_6^{3-}$ -containing mixtures became white turbid, and droplets were clearly visible
 180 under the microscope.
 181



182
 183 **Figure 2.** (a) Schematic illustration of the redox reaction network underlying dynamic and reversible formation and
 184 dissolution of $\text{Fe}(\text{CN})_6^{4-}/\text{pLys}$ coacervate droplets. (b) Optical observation of droplet dissolution by $\text{S}_2\text{O}_8^{2-}$ addition to
 185 $\text{Fe}(\text{CN})_6^{4-}/\text{pLys}$ coacervates dispersion and droplet formation by GSH addition. Scale bars: 10 μm . Insets show
 186 photographs of the corresponding turbid suspensions, or the clear solution. (c) Formation of $\text{Fe}(\text{CN})_6^{4-}/\text{pLys}$ coacervate
 187 droplets induced by addition of 1 equivalent of NADH at pH 4, but not at pH 7.4. (d) Same as (c), but induced by
 188 addition of 1 equivalent of GSH, which proceeds at pH 7.4, but not at pH 4. (e) Alternating additions of GSH and
 189 $\text{S}_2\text{O}_8^{2-}$ at pH 7.4 show that condensation and dissolution are both reversible and that the system can be switched
 190 multiple times between a compartmentalized droplet state and a single-phase homogeneous solution.

191 The oxidation reaction showed a clear pH dependence (Fig. 2c,d). We were able to use a
192 stoichiometric amount of GSH to turn a homogeneous ferricyanide solution into a dispersion of
193 ferrocyanide droplets in the presence of pLys within 5 minutes in neutral conditions (pH 7.4, Fig.
194 2b,d), while no conversion occurred under acidic conditions (pH 4). When using NADH as
195 reducing agent, almost no conversion of the same homogeneous ferricyanide solution with pLys
196 could be observed in neutral conditions (pH 7.4, Fig. 2c), while complete conversion into
197 ferrocyanide droplets was observed within 15 minutes under acidic conditions (pH 4). In both
198 cases, with GSH and NADH, a stoichiometric amount of $S_2O_8^{2-}$ completely dissolved a dispersion
199 of $Fe(CN)_6^{4-}$ droplets, converting $Fe(CN)_6^{4-}$ back into $Fe(CN)_6^{3-}$ within ten minutes. Fig. 2e
200 illustrates the remarkable reversibility of this process: droplets could be generated and dissolved
201 up to eight times, and we were able to carry out identical transitions when starting from either
202 $Fe(CN)_6^{4-}$ or $Fe(CN)_6^{3-}$. After eight cycles, the system loses its ability to condense into droplets,
203 which is mainly caused by accumulation of the waste products from GSH or NADH and $S_2O_8^{2-}$.
204 The level of redox control over droplet generation shown in Figure 2 has not been achieved before
205 and holds great promise for the development of dynamic protocell models.

206 For use of these ferricyanide coacervates as potential oxidizing hubs in which oxidation
207 reactions could be localized, it is important to know where the redox reactions utilized in Fig. 2
208 take place. We can take advantage of the fluorescence of common redox-active metabolites such
209 as NADPH, in combination with the observed pH dependence, to monitor the conversion ferri- and
210 ferrocyanide. We incubated ferricyanide/(Arg)₁₀ coacervates (8 mM ferricyanide/24 mM Arg) with
211 2 mM NADPH at neutral pH and observed clear NADPH fluorescence inside the coacervates,
212 indicating that NADPH is sequestered by the coacervates (Supplementary Fig. 7). At this pH, the
213 reduction of ferricyanide by NADPH is suppressed (Fig. 2c), which allows for equilibration and
214 focusing of the microscope. We then decreased the outer pH by addition of a fixed amount of acid

215 and monitored how the redox reaction progressed and led to the rapid disappearance of the
216 fluorescence of NADPH within 2 min. (Supplementary Fig. 7). Interestingly, the fluorescence
217 intensity first disappeared from the center of the coacervate droplets (Supplementary Fig. 7),
218 indicating that the oxidation of NADPH to non-fluorescence NADP^+ by ferricyanide took place
219 predominantly inside the droplets instead of in solution,¹⁸ in which case an exchange of
220 NADPH/ NADP^+ and reduction of fluorescence at the droplet interface would be expected. Taken
221 together, these data show our ferricyanide-based coacervates are redox-active compartments that
222 can locally oxidize sequestered metabolites.

223

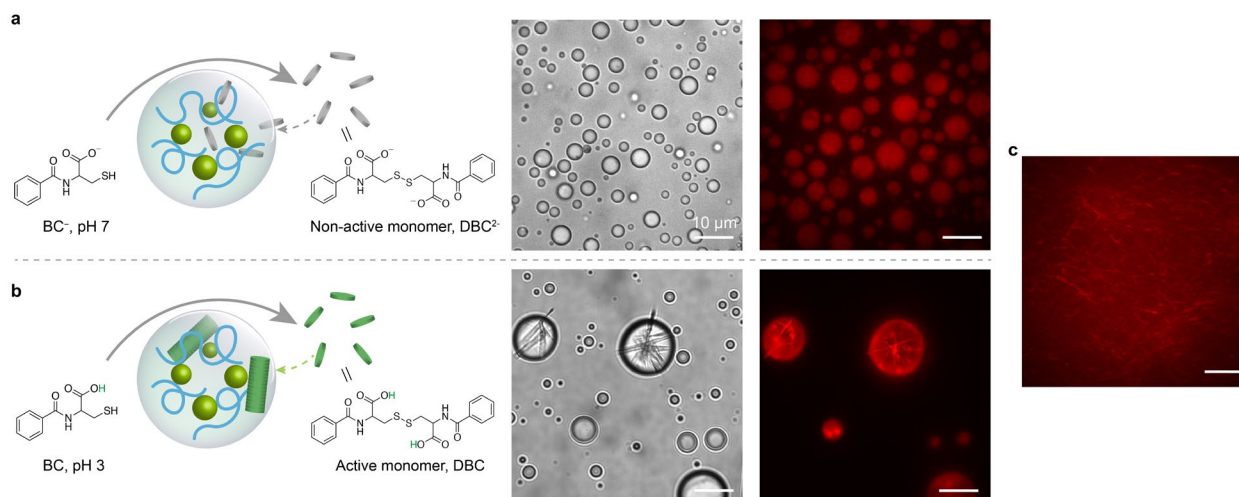
224 **Fiber self-assembly inside ferricyanide-based coacervates**

225 We further investigated if the redox activity of ferricyanide-based coacervates could lead to
226 spatially controlled higher order assembly. Self-assembly of filaments inside or at the periphery of
227 (proto)cellular compartments is key to many transport processes, locomotion and division.^{39,40}
228 Spatially controlled assembly of analogous model filaments in cell-like compartments is therefore
229 an interesting goal in protocell and synthetic cell research.⁴⁰⁻⁴² We selected an amino acid
230 derivative benzoyl cysteine as precursor for filaments (Fig. 3). *N,N'*-dibenzoyl-L-cystine (DBC) is
231 a well-known redox-active supramolecular gelator,^{43,44} which has been used to make filaments in
232 aqueous solution at low pH. To create the precursor form, we reduced the water soluble DBC^{2-} at
233 pH 7 with 1 equivalent of dithiothreitol (DTT) to give non-active monomer *N*-benzoyl-L-cysteine
234 (BC^-), which is highly soluble at both high and low pH and does not stack to form fibers.

235 We flushed a solution of BC^- (with dye Nile red) in a microchamber containing
236 ferricyanide/ $(\text{Arg})_{10}$ coacervates (final concentration: 10 mM BC^- , 4 mM ferricyanide, 12 mM
237 $(\text{Arg})_{10}$ (monomer basis)) at pH 7. Upon addition of the coacervates, we observed a gradual increase
238 in the total fluorescent intensity inside coacervates, as newly formed non-active monomer 2-

239 charged DBC^{2-} , which weakly binds to Nile red, partitioned in the coacervates (Fig. 3a). At this
 240 pH, no fibers are formed, and the non-active DBC^{2-} monomers are distributed homogeneously
 241 inside the coacervates. We note that ferricyanide/peptide coacervates without DBC^{2-} do not
 242 sequester Nile red (Supplementary Fig. 4h). Upon addition of BC to an aqueous dispersion of
 243 ferricyanide/ $(\text{Arg})_{10}$ coacervates at pH 3 (below the pK_a of the carboxylate groups of DBC, $\text{pK}_a \sim$
 244 3.6),⁴⁴ we observed oxidized, bright fluorescent DBC filaments assembled into shells around the
 245 coacervate droplets, and several bundles of filaments present inside the droplets (Fig. 3b). The
 246 bundled filaments inside the coacervates are clearly visible in transmission, and are strongly stained
 247 by Nile red. These bundles can be seen to pierce the interface of the coacervate droplets. In control
 248 with ferricyanide but without polycations, we observed a fiber dispersion without clear bundling
 249 or formation of shells (Fig. 3c).

250



251

252 **Figure 3.** (a) Confocal micrographs of ferricyanide/ $(\text{Arg})_{10}$ protocells (with dye, Nile red), time series of representative
 253 protocells after addition of BC^- . (b) Confocal micrographs of ferricyanide/ $(\text{Arg})_{10}$ protocells (with dye, Nile red) after
 254 addition of BC. (c) Confocal micrographs of fiber formation after adding ferricyanide into BC solution.

255 A similar type of interfacial filament assembly has been observed for actin filaments and
256 peptide-based pLys/pGlu coacervates before.⁴¹ We also observed that different peptides lead to
257 altered fiber assembly: in the case of ferricyanide/(Lys(Me)₃)₂₀ and ferricyanide/(Lys(Me)₃)₃₀
258 coacervates, the fibers preferentially localized inside and at the interface of the coacervates
259 (Supplementary Fig. 8a-b). Interestingly, in the case of ferricyanide/(Lys)₃₀ coacervates, the fibers
260 did not remain confined inside the coacervates, but grew out into the surrounding environment,
261 giving an aster-like shape (Supplementary Fig. 8c). In short, these findings show that ferricyanide
262 coacervates can drive the formation of self-assembled filaments via oxidation of the filament
263 precursors.

264

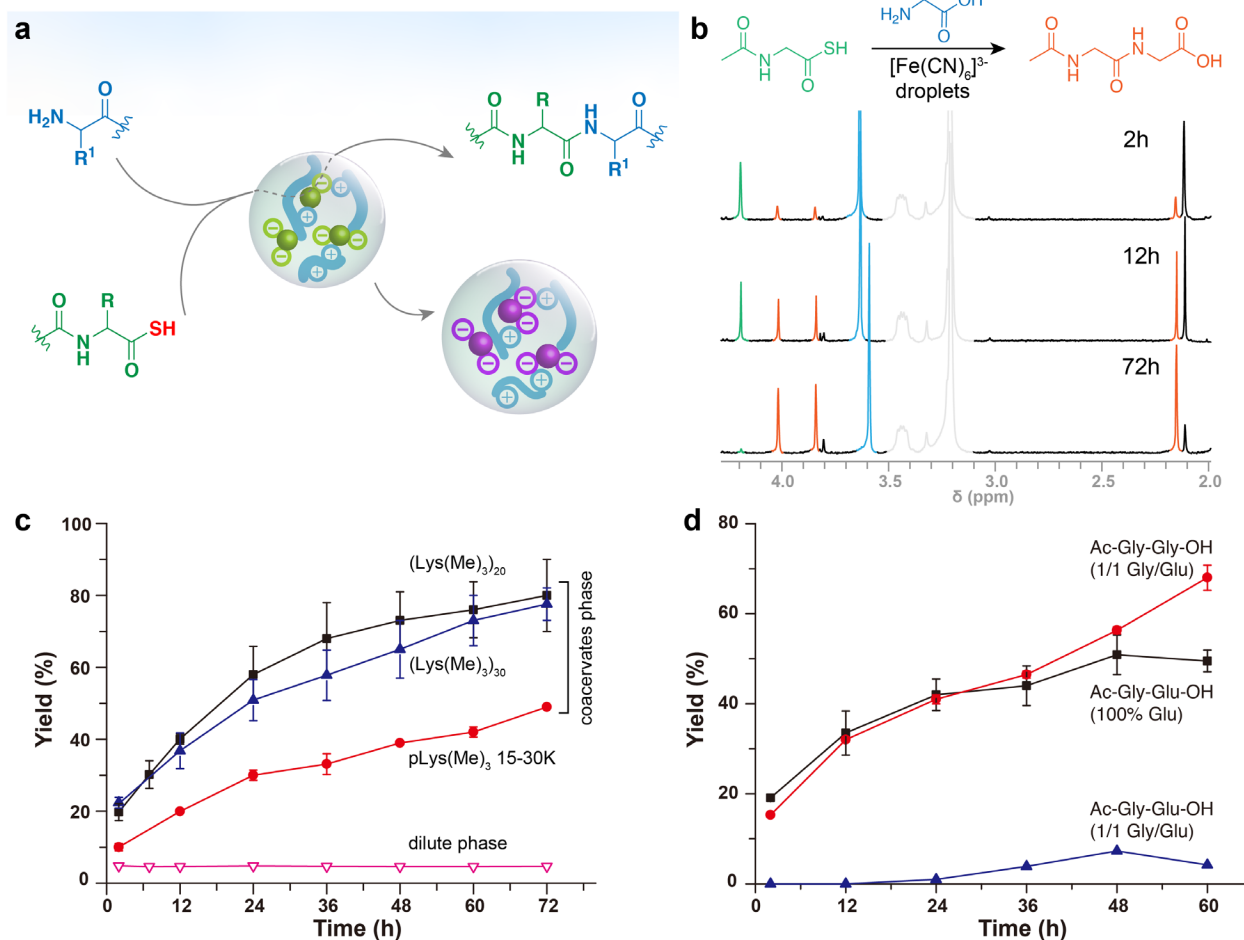
265 **Amide bond formation through amino thioacid oxidation in coacervate protocells**

266 Having established the potential of ferricyanide-based coacervates as oxidizing hubs for redox-
267 active guest molecules, we sought to use the oxidizing potential to synthesize peptides by
268 catalyzing the formation of amide bonds. Ferricyanide has been described as a prebiotically
269 abundant oxidizing agent,³³ and has been used to activate amino thioacids by oxidation to facilitate
270 the formation of an amide bond upon reaction with nucleophilic aminonitriles and amino acids.⁶⁻
271 ^{9,34} However, the oxidative aminoacylation of thioacids is usually performed with high reactant and
272 ferricyanide concentrations (sometimes close to 100 mM), which could have been difficult to reach
273 everywhere on Early Earth. Therefore, the highly concentrated ferricyanide coacervate droplets
274 could be interesting model compartments for prebiotic amide bond formation (Fig. 4a). As a proof
275 of principle, we first prepared ferricyanide coacervate droplets by direct mixing of aqueous
276 solutions of ferricyanide and trimethylated poly-L-lysine (pLys(Me)₃) at charge stoichiometry. The
277 pLys(Me)₃ was chosen to avoid the ϵ -coupling of Lys-NH₂. To study the amide bond formation in
278 coacervate droplets, we incubated *N*-acetyl-glycine thioacid (Ac-Gly-SH) (8 mM) with Gly (3 eq.)

279 in ferricyanide (1 eq.)/ pLys(Me)₃ coacervates dispersion at pH 9. The consumption of Ac-Gly-SH
280 and formation of the ligation product Ac-Gly-Gly-OH was monitored with ¹H NMR (Fig. 4b).

281 Interestingly, we found a yield of Ac-Gly-Gly-OH of up to 80% after 3 days in the presence
282 of coacervates, while in dilute phase at most 5% of ligation product was observed. In controls with
283 peptides but without ferricyanide, we found no ligation product (Supplementary Fig. 9), and also
284 in the presence of ferrocyanide/pLys coacervate droplets, no ligation product was observed
285 (Supplementary Fig. 10). The significantly higher yield in the presence of coacervates can be
286 attributed to the high local ferricyanide concentration inside coacervate droplets and implies that
287 the ligation reaction takes place predominantly inside the coacervates. Ferricyanide-based
288 coacervate droplets can thus act as microreactors that enhance the rates of oxidative aminoacylation.
289 We found that the ligation reaction was most enhanced in droplets formed from shorter peptides,
290 (Lys(Me)₃)₂₀ and (Lys(Me)₃)₃₀, compared to longer pLys(Me)₃ (Fig. 4c). We attribute this to the
291 lower multivalency of the polycation, which results in weaker complexation with the ferricyanide,
292 making it more available for the reaction with the amino thioacids.

293 From an origins of life perspective, it is interesting to explore the selectivity of aminoacylation
294 when more than one amino acid can react with an available amino thioacid inside coacervate
295 droplets. Instead of only glycine (Gly), stoichiometric (1:1) competition reactions between glycine
296 and glutamic acid (Glu), Alanine (Ala), and Phenylalanine (Phe) were investigated. All competition
297 reactions demonstrated a significant selectivity for one of the ligation products at pH 9
298 (Supplementary Table 1). For example, when we added both glycine (12 mM) and glutamic acid
299 (12 mM) to ferricyanide-based droplets (8 mM ferricyanide) containing Ac-Gly-SH (8 mM), we
300 observed a strong selectivity for peptide ligation with glycine. Glutamic acid alone yields the Ac-
301 Gly-Glu-OH dipeptide in similar yields as glycine (Fig. 4d, Supplementary Fig. 11a), but when



302

303 **Figure 4.** Peptide bond formation in ferricyanide-based droplets. (a) Schematic illustration of ferricyanide-based
 304 droplets as microreactors for peptide ligation in water. (b) ¹H NMR spectrum showing the peptide ligation reaction of
 305 *N*-acetyl-glycine thioacid Ac-Gly-SH (8mM, green) and Gly-OH (3 equiv., blue) with ferricyanide/plys(Me)₃ (gray)
 306 coacervates (1 equiv., pH 9, room temperature) to yield Ac-Gly-Gly-OH (orange). (c) Plot of % ligation products vs
 307 time for peptide ligation reaction in dilute phase or ferricyanide-based coacervate droplets. (d) Plot of selective peptide
 308 bond formation within coacervate droplets.

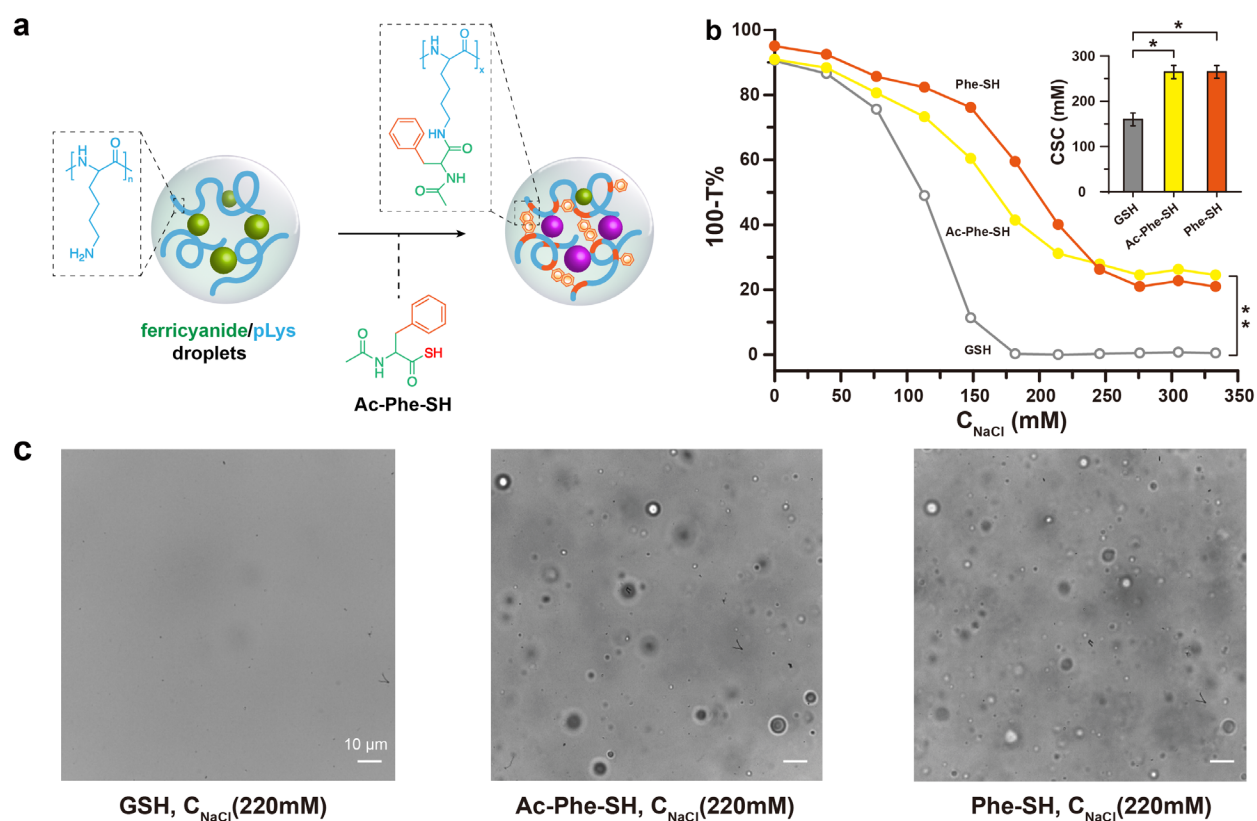
309

310 glycine and glutamic acid were incubated together in a 1:1 ratio with Ac-Gly-SH in
 311 (Lys(Me)₃)₂₀/ferricyanide coacervates, more than 90% of the ligation products was Ac-Gly-Gly-
 312 OH (Fig. 4d, Supplementary Fig. 11b). Glycine thus outcompeted glutamic acid very effectively
 313 in the ligation process. We reasoned that the activity of glycine inside coacervates is higher than
 314 glutamic acid. Although glycine and glutamic acid have similar nucleophilicities,⁴⁵ glutamic acid

315 is bound more strongly to the cationic lysine residues inside the coacervate and therefore has a
316 lower activity. As a result, glycine reacts faster than glutamic acid inside the coacervate
317 environment and the outcome we observe is an example of kinetic pathway selection, caused by
318 the local protocell environment. Likewise, we observed selective incorporation of glycine in
319 mixtures with alanine (83% Gly/17% Ala) and phenylalanine (78% Gly/22% Phe) (Supplementary
320 Table 1), because the latter have a slightly stronger interaction with the peptide backbone in the
321 coacervates. Alanine is incorporated with slight preference over glutamic acid (60% Ala/40% Glu),
322 but surprisingly, glutamic acid is incorporated more very slightly effectively than phenylalanine
323 (63% Glu/37% Phe).

324 The products of the above reactions with simple amino (thio)acids are small molecules that
325 interact only weakly with the coacervates. Therefore, they can quickly escape the protocell and the
326 evolutionary advantage for the protocells is limited. To establish a feedback between the formation
327 of amide bonds inside protocells and protocell fitness, we sought to retain the reaction product
328 inside the coacervates. We tested if the scaffold peptides used to form the coacervates could
329 themselves react as nucleophiles with oxidized aminothioacids. We added Ac-Phe-SH or Phe-SH
330 (4 mM) to ferricyanide (4 mM)/ pLys (12 mM) droplets, leading to ϵ -NH₂ ligation of the protocell
331 building blocks (pLys) (Fig. 5a, Supplementary Fig. 12). Anchoring of the aromatic phenylalanine
332 to the pLys scaffold makes the coacervate interior more hydrophobic, and leads to additional
333 cation- π interactions between the coacervate components, both of which result in an expected
334 increase in salt resistance.²⁷ Indeed, we found that ferricyanide/pLys-g-Phe coacervates remain
335 stable far beyond the CSC of the original ferricyanide/pLys coacervates. Fig. 5b shows the turbidity
336 of the coacervates for increasing the salt concentrations. In the control sample, to which we added
337 GSH (4 mM) instead of an amino thioacid to reduce the ferricyanide, the turbidity decreases and

338 reaches background levels around 180 mM NaCl, where all droplets had disappeared completely
 339 (Fig. 5c). In contrast, when Ac-Phe-SH/Phe-SH was added and reacted with the ϵ -NH₂ of pLys,
 340 the turbidity transition shifted to a significantly higher salt concentration and the absolute intensity
 341 of the plateau at high salt concentration was higher (Fig. 5b). Even at high salt concentrations (220
 342 mM), above the original CSC, microscope images show the presence of gel-like droplets, which
 343 do not fuse (Fig. 5c). These condensates have an increased salt resistance and a more gel-like
 344 consistency as a result of the attachment of an aromatic residue to the pLys side chains.
 345



346

347 **Figure 5.** (a) Schematic representation of pLys ϵ -NH₂ ligation in coacervates. (b) Salt resistance of coacervates with
 348 Ac-Phe-SH/Phe-SH ligation with droplets building blocks (pLys). Insets show the significantly different of the
 349 corresponding CSC, or the turbidity plateau. (c) Optical microscope images illustrating samples corresponding to the
 350 high salt concentration (220 mM) points in (b).

351 **Conclusion**

352 In summary, we developed a protocell model based on prebiotically relevant ferricyanide as redox-
353 active species. Membrane-free droplet compartments were spontaneously assembled in the presence
354 of short cationic peptides and the assembly of ferri/ferrocyanide-peptide droplets can be regulated
355 by redox chemistry and salt concentration. Ferricyanide-peptide droplets can act as oxidizing hubs
356 for metabolites, such as NAD(P)H and GSH, filament stacking element like benzoyl cysteine, and
357 amino thioacids as potential prebiotic precursors of amino acids. We demonstrate that the oxidation
358 of amino thioacids by ferricyanide coacervates can be used to drive aminoacylation, resulting in
359 the formation of new peptide bonds. The amino acid ligation is enhanced in coacervate dispersions
360 compared to the surrounding dilute phase due to the local high ferricyanide concentration. The
361 coacervate environment imposes a selection pressure that results in kinetic pathway selection and
362 a strong, preferential incorporation of certain amino acids. Finally, this strategy can be used to
363 create self-reinforcing coacervates, in which hydrophobic amino acid residues are ligated to the
364 coacervate building blocks and enhance their stability. Our results show that prebiotically relevant
365 ferricyanide-based coacervate protocells are versatile oxidizing hubs that exist in aqueous solution,
366 in which metabolites can be sequestered and peptides synthesized. These results provide an
367 important step towards prebiotically plausible integration of chemical processes in cellular
368 compartments.

369

370 **Methods**

371 A full description of materials and methods used in this work is given in the Supplementary
372 Information.

373

374 **Acknowledgements**

375 This work was financially supported by the European Research Council (ERC) under grant number
376 851963. The authors would like to thank Karina Nakashima for synthesis of the *N*-acetyl glycine
377 thioacid and helpful discussions about the project goals, Haibin Qian for preliminary experiments
378 on EDC-mediated amide bond formation in pGlu/pLys(Me)₃ coacervates and the methylation
379 protocol for pLys, and Tiemei Lu for help with preparing the methylated pLys.

380

381 **Additional information**

382 Supplementary information accompanies this paper.

383

384 **Author information**

385 **Corresponding authors**

386 *Email: e.spruijt@science.ru.nl

387 *Email: junyouwang@ecust.edu.cn

388

389 **Competing interests**

390 The authors declare no competing financial interests.

391

392 **References**

- 393 1. Nissen, P., Hansen, J., Ban, N., Moore, P. B. & Steitz, T. A. The Structural Basis of Ribosome Activity in
394 Peptide Bond Synthesis. *Science* **289**, 920–930 (2000).
- 395 2. Goswami, A. & Lanen, S. G. V. Enzymatic strategies and biocatalysts for amide bond formation: tricks of the
396 trade outside of the ribosome. *Mol. Biosyst.* **11**, 338–353 (2015).
- 397 3. Joyce, G. F. & Szostak, J. W. Protocells and RNA Self-Replication. *Cold Spring Harb. Perspect. Biol.* **10**,
398 a034801 (2018).
- 399 4. Li, M., Huang, X., Tang, T.-Y. D. & Mann, S. Synthetic cellularity based on non-lipid micro-compartments and
400 protocell models. *Curr. Opin. Chem. Biol.* **22**, 1–11 (2014).

- 401 5. Abbas, M., Lipiński, W. P., Wang, J. & Spruijt, E. Peptide-based coacervates as biomimetic protocells. *Chem.*
402 *Soc. Rev.* **50**, 3690–3705 (2021).
- 403 6. Maurel, M.-C. & Orgel, L. E. Oligomerization of α -Thioglutamic Acid. *Orig. Life Evol. Biosph.* **30**, 423–430
404 (2000).
- 405 7. Canavelli, P., Islam, S. & Powner, M. W. Peptide ligation by chemoselective aminonitrile coupling in water.
406 *Nature* **571**, 546–549 (2019).
- 407 8. Okamoto, R. *et al.* Regioselective α -Peptide Bond Formation Through the Oxidation of Amino Thioacids.
408 *Biochemistry* **58**, 1672–1678 (2019).
- 409 9. Liu, R. & Orgel, L. E. Oxidative acylation using thioacids. *Nature* **389**, 52–54 (1997).
- 410 10. McLean, E. B. & Lee, A.-L. Golden potential. *Nat. Chem.* **11**, 760–761 (2019).
- 411 11. Sokolova, E. *et al.* Enhanced transcription rates in membrane-free protocells formed by coacervation of cell
412 lysate. *Proc. Natl. Acad. Sci.* (2013) doi:10.1073/pnas.1222321110.
- 413 12. Drobot, B. *et al.* Compartmentalised RNA catalysis in membrane-free coacervate protocells. *Nat. Commun.* **9**,
414 3643 (2018).
- 415 13. Poudyal, R. R. *et al.* Template-directed RNA polymerization and enhanced ribozyme catalysis inside
416 membraneless compartments formed by coacervates. *Nat. Commun.* **10**, 490 (2019).
- 417 14. Mason, A. F. *et al.* Mimicking Cellular Compartmentalization in a Hierarchical Protocell through Spontaneous
418 Spatial Organization. *ACS Cent. Sci.* **5**, 1360–1365 (2019).
- 419 15. Altenburg, W. J. *et al.* Programmed spatial organization of biomacromolecules into discrete, coacervate-based
420 protocells. *Nat. Commun.* **11**, 6282 (2020).
- 421 16. Abbas, M., Lipiński, W. P., Nakashima, K. K., Huck, W. T. S. & Spruijt, E. Short peptide synthon for liquid-
422 liquid phase separation. *Nat. Chem.* doi:10.1038/s41557-021-00788-x.
- 423 17. Koga, S., Williams, D. S., Perriman, A. W. & Mann, S. Peptide–nucleotide microdroplets as a step towards a
424 membrane-free protocell model. *Nat. Chem.* **3**, 720–724 (2011).
- 425 18. Donau, C. *et al.* Active coacervate droplets as a model for membraneless organelles and protocells. *Nat.*
426 *Commun.* **11**, 5167 (2020).
- 427 19. Cakmak, F. P., Choi, S., Meyer, M. O., Bevilacqua, P. C. & Keating, C. D. Prebiotically-relevant low polyion
428 multivalency can improve functionality of membraneless compartments. *Nat. Commun.* **11**, 5949 (2020).
- 429 20. Lu, T. & Spruijt, E. Multiphase Complex Coacervate Droplets. *J. Am. Chem. Soc.* **142**, 2905–2914 (2020).
- 430 21. Mountain, G. A. & Keating, C. D. Formation of Multiphase Complex Coacervates and Partitioning of
431 Biomolecules within them. *Biomacromolecules* **21**, 630–640 (2020).
- 432 22. Zhang, Y. *et al.* Giant Coacervate Vesicles As an Integrated Approach to Cytomimetic Modeling. *J. Am. Chem.*
433 *Soc.* **143**, 2866–2874 (2021).
- 434 23. Nakashima, K. K., van Haren, M. H. I., André, A. A. M., Robu, I. & Spruijt, E. Active coacervate droplets are
435 protocells that grow and resist Ostwald ripening. *Nat. Commun.* **12**, 3819 (2021).
- 436 24. Love, C. *et al.* Reversible pH-Responsive Coacervate Formation in Lipid Vesicles Activates Dormant
437 Enzymatic Reactions. *Angew. Chem. Int. Ed.* **59**, 5950–5957 (2020).
- 438 25. Last, M. G. F., Deshpande, S. & Dekker, C. pH-Controlled Coacervate–Membrane Interactions within
439 Liposomes. *ACS Nano* **14**, 4487–4498 (2020).
- 440 26. Deng, N.-N. & Huck, W. T. S. Microfluidic Formation of Monodisperse Coacervate Organelles in Liposomes.
441 *Angew. Chem. Int. Ed.* **56**, 9736–9740 (2017).
- 442 27. Lu, T., Nakashima, K. K. & Spruijt, E. Temperature-Responsive Peptide–Nucleotide Coacervates. *J. Phys.*
443 *Chem. B* **125**, 3080–3091 (2021).
- 444 28. Martin, N. *et al.* Photoswitchable Phase Separation and Oligonucleotide Trafficking in DNA Coacervate
445 Microdroplets. *Angew. Chem. Int. Ed.* **58**, 14594–14598 (2019).
- 446 29. Aumiller, W. M. & Keating, C. D. Phosphorylation-mediated RNA/peptide complex coacervation as a model
447 for intracellular liquid organelles. *Nat. Chem.* **8**, 129–137 (2016).
- 448 30. Nakashima, K. K., Baaij, J. F. & Spruijt, E. Reversible generation of coacervate droplets in an enzymatic
449 network. *Soft Matter* **14**, 361–367 (2018).
- 450 31. Deshpande, S. *et al.* Spatiotemporal control of coacervate formation within liposomes. *Nat. Commun.* **10**, 1800
451 (2019).
- 452 32. Bungenberg de Jong, H. G. & Kruyt, H. R. Coacervation (Partial miscibility in colloid systems). *Proc Kon Ned*
453 *Akad Wet* **32**, 849–856 (1929).
- 454 33. Keefe, A. D. & Miller, S. L. Was ferrocyanide a prebiotic reagent? *Orig. Life Evol. Biosph.* **26**, 111–129 (1996).
- 455 34. Leman, L., Orgel, L. & Ghadiri, M. R. Carbonyl Sulfide-Mediated Prebiotic Formation of Peptides. *Science*
456 **306**, 283–286 (2004).

- 457 35. Coggins, A. J. & Powner, M. W. Prebiotic synthesis of phosphoenol pyruvate by α -phosphorylation-controlled
458 triose glycolysis. *Nat. Chem.* **9**, 310–317 (2017).
- 459 36. Sokalingam, S., Raghunathan, G., Soundarajan, N. & Lee, S.-G. A Study on the Effect of Surface Lysine to
460 Arginine Mutagenesis on Protein Stability and Structure Using Green Fluorescent Protein. *PLOS ONE* **7**,
461 e40410 (2012).
- 462 37. Choi, E.-Y. *et al.* Electrochemical Characteristics of Polyelectrolyte Brushes with Electroactive Counterions.
463 *Langmuir* **23**, 10389–10394 (2007).
- 464 38. Wang, J., Cohen Stuart, M. A. & van der Gucht, J. Phase Diagram of Coacervate Complexes Containing
465 Reversible Coordination Structures. *Macromolecules* **45**, 8903–8909 (2012).
- 466 39. Miyazaki, M., Chiba, M., Eguchi, H., Ohki, T. & Ishiwata, S. Cell-sized spherical confinement induces the
467 spontaneous formation of contractile actomyosin rings in vitro. *Nat. Cell Biol.* **17**, 480–489 (2015).
- 468 40. te Brinke, E. *et al.* Dissipative adaptation in driven self-assembly leading to self-dividing fibrils. *Nat.*
469 *Nanotechnol.* **13**, 849–855 (2018).
- 470 41. McCall, P. M. *et al.* Partitioning and Enhanced Self-Assembly of Actin in Polypeptide Coacervates. *Biophys. J.*
471 **114**, 1636–1645 (2018).
- 472 42. Fanalista, F., Deshpande, S., Lau, A., Pawlik, G. & Dekker, C. FtsZ-Induced Shape Transformation of
473 Coacervates. *Adv. Biosyst.* **2**, 1800136 (2018).
- 474 43. Boekhoven, J., Hendriksen, W. E., Koper, G. J. M., Eelkema, R. & Esch, J. H. van. Transient assembly of active
475 materials fueled by a chemical reaction. *Science* **349**, 1075–1079 (2015).
- 476 44. Wojciechowski, J. P., Martin, A. D. & Thordarson, P. Kinetically Controlled Lifetimes in Redox-Responsive
477 Transient Supramolecular Hydrogels. *J. Am. Chem. Soc.* **140**, 2869–2874 (2018).
- 478 45. Brotzel, F. & Mayr, H. Nucleophilicities of amino acids and peptides. *Org. Biomol. Chem.* **5**, 3814–3820
479 (2007).

480

Supplementary information

Selective amide bond formation in redox-active coacervate protocells

Jiahua Wang,^[a] Manzar Abbas,^[a] Junyou Wang^{*[b]} and Evan Spruijt^{*[a]}

^[a] Radboud University, Institute for Molecules and Materials, Heyendaalseweg 135, 6525 AJ Nijmegen, the Netherlands

^[b] State Key Laboratory of Chemical Engineering and Shanghai Key Laboratory of Multiphase Materials Chemical Engineering, East China University of Science and Technology, Shanghai 200237, China

*Email: e.spruijt@science.ru.nl, or: junyouwang@ecust.edu.cn

Materials and methods

Materials

Poly-L-lysine hydrobromide (pLys, 15–30 kDa), potassium ferricyanide, potassium ferrocyanide, glutathione (GSH), DL-dithiothreitol (DTT), tris(hydroxymethyl)aminomethane (Tris), pyranine, and sodium chloride were purchased from Sigma Aldrich and used without further purification. Short polycations (Lys)₁₀, (Lys)₂₀, (Lys)₃₀, (Arg)₁₀ were purchased from Alamanda Polymers. Nicotinamide adenine dinucleotide (NADH) and nicotinamide adenine dinucleotide phosphate (NADPH) were purchased from Roche. The fluorescently labeled oligonucleotides poly-A₁₅ (Cy5-A₁₅), Poly-rU₁₅ (rU₁₅-Cy3Sp) were purchased from Integrated DNA Technologies (IDT).

Coacervate formation

Samples for turbidity measurements were prepared directly into 96-well plates, by adding, respectively, Milli-Q water, Tris buffer (pH 7.4, 50 mM), pLys, and ferricyanide or ferrocyanide to a total volume of 100 μ L. Mixing was done by gentle pipetting (3 \times) before each measurement. Samples for the microscopy experiments were prepared in microcentrifuge tubes. After addition of the substrate, a 20 μ L aliquot was immediately taken for imaging on a glass slide.

Turbidity measurements

Turbidity measurements were performed in triplicate using a Berthold Tristar (2) LB 942 microplate reader. The temperature was kept constant at $25 \pm 1^\circ\text{C}$. The absorbance was measured at 520 nm, where none of the mixture components absorbed significantly. The absorbance of a well filled with the same volume of water was used as a blank. Samples were shaken for 5 s before every readout. The critical point was determined by extrapolating the first-order derivative at the inflection point to zero turbidity. Note that this critical salt concentration does not take into account ions from other sources than the added NaCl, and the actual critical ionic strength may be slightly higher.

Ferricyanide and ferrocyanide partitioning

In a typical procedure, the coacervates dispersion was centrifuged in an Eppendorf tube at 3000x g until the dilute phase was transparent under microscope, the coacervate phase had sedimented to the bottom of the cell. The concentration of the ferricyanide/ferrocyanide in the dilute phase was quantitatively analyzed with Uv-vis at wavelength of 320 nm and 420 nm (Supplementary Fig. 5). We measured the volume of the top (dilute) solution and calculated the ferricyanide/ferrocyanide

concentrations of the top solution from the standard curve, the volume and the moles of ferricyanide /ferrocyanide in coacervate phase can be calculated from the total feed, then the ferricyanide and ferrocyanide concentrations inside the coacervate phase can be obtained.

Confocal fluorescence microscopy

Optical and fluorescence microscopy images were recorded on an Olympus UIS2 microscope, equipped with a motorized stage (Prior, Optiscan II). Fluorescent images were recorded with an EMCCD camera (Andor, iXon), using illumination from a mercury lamp, an excitation filter of 482/18 nm (Semrock BrightLine) and an emission filter of 525/45 nm (Semrock BrightLine). Samples were loaded into the wells of PLL-g-PEG-functionalized *Ibidi* μ -slides and closed with a lid (microscopy chambers).

Microscopy chambers preparation

The *Ibidi* μ -slides used for imaging were functionalized with PLL-g-PEG to minimize wetting and spreading of the coacervate droplets. Each slide was first activated by oxygen plasma treatment (Diener electronic, Femto). The PLL-g-PEG (0.01 mg/mL in 10 mM HEPES buffer, pH 7.4) solution was added into each well and incubated at room temperature for 1 h. After that, the glass slides were cleaned by rinsing (3 times with 10 mM HEPS, pH 7.4, 3 times with MQ). The slides were dried by using compressed air.

NMR measurements

Nuclear Magnetic Resonance (NMR) spectra were measured on a Bruker-AVANCE III 400 MHz spectrometer.

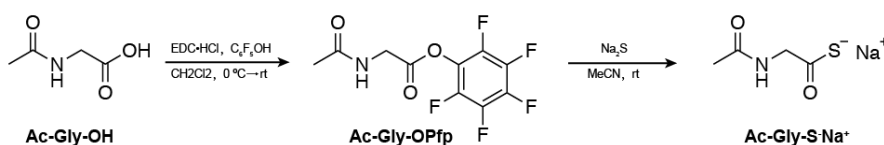
Mass spectrometry

Mass spectra were obtained from a Thermo Scientific™ LCQ Fleet™ ion trap mass spectrometer with Gemini-NX C18 110A 150 x 2.0 mm column and JEOL Accurate Time of Flight (ToF) instruments, both using linear ion trap electrospray ionisation (ESI).

Synthesis of trimethylated oligolysine and poly-L-lysine

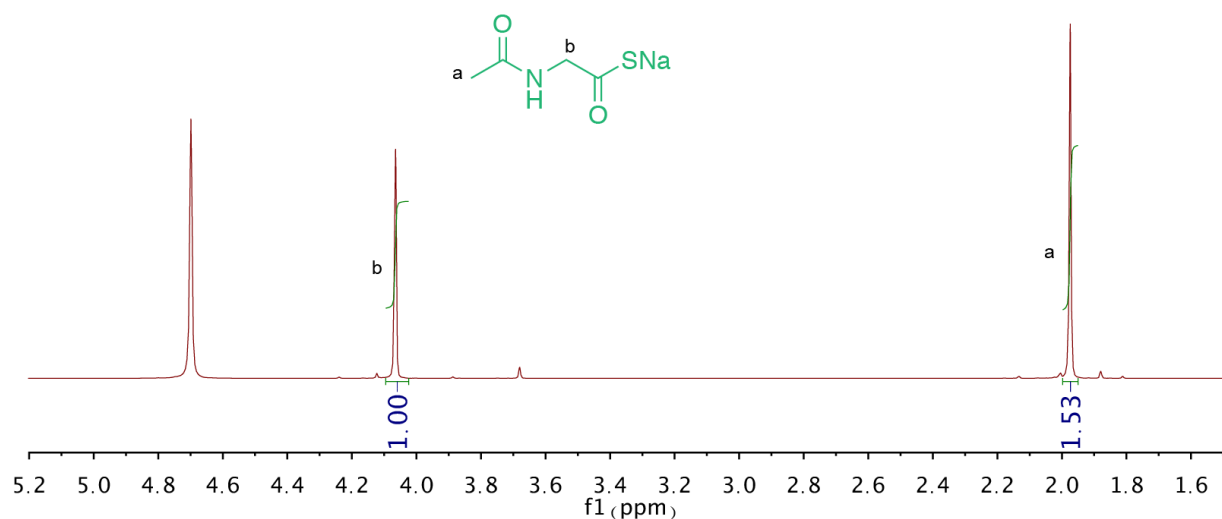
Trimethylated oligolysines (Lys(Me)₃)_n and poly-L-lysine (pLys(Me)₃) were prepared from (Lys)_n and pLys, according to literature methods.³ Briefly, 2 mL DMS was added to 50 mg (Lys)_n, in 20 mL H₂O and 6 mL ethanol. The pH was adjusted to 9.5 and maintained by the addition of 1 M NaOH. The reaction was considered complete when the pH remained nearly constant. The pLys(Me)₃ was further purified by dialysis against 2 times 1 L of a 2 M NaCl aqueous solution and subsequently, 3 times 1 L of water in a dialysis membrane (MWCO, 3500). After that, the residue was freeze-dried to yield a white powder.

Synthesis of sodium 2-acetamidoethanethioate Ac-Gly-S⁻Na⁺

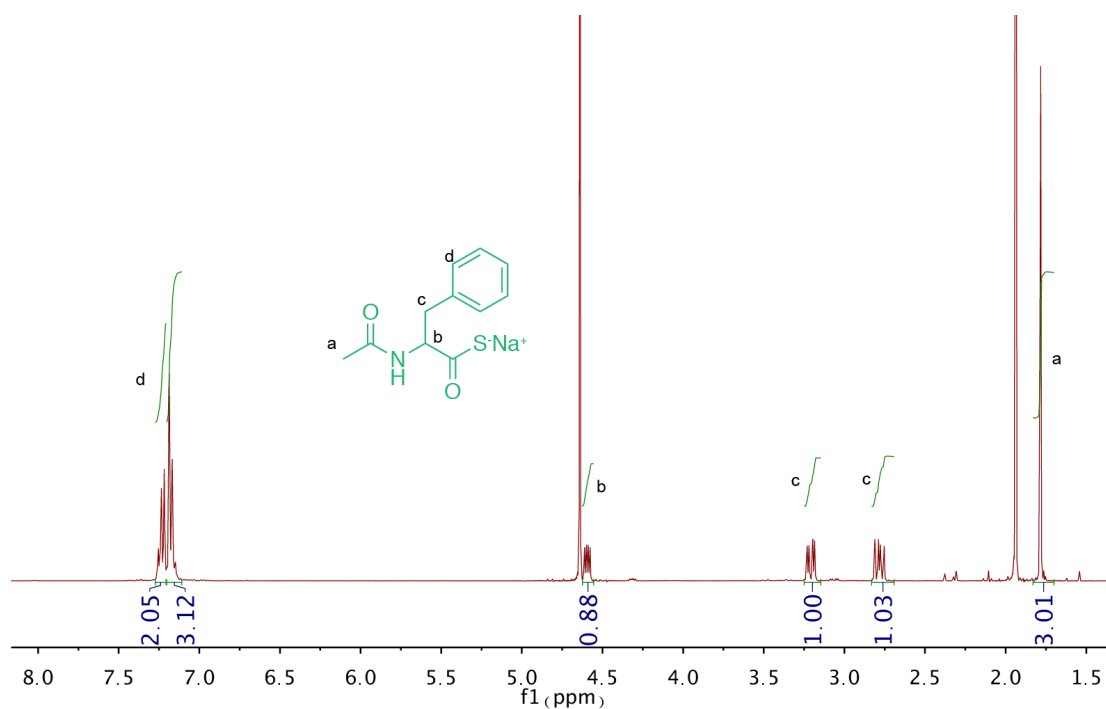


Ac-Gly-S⁻Na⁺, Ac-Phe-S⁻Na⁺ and Phe-SH were synthesized according to literature methods (Supplementary Fig. 1-3).¹⁻² In brief, for **Ac-Gly-S⁻Na⁺**, *N*-(3-Dimethylaminopropyl)-*N'*-ethylcarbodiimide hydrochloride (EDC·HCl) (3.45 g, 18.00 mmol) was added to a stirring solution of *N*-acetylglycine **Ac-Gly-OH** (943 mg, 6.00 mmol) and pentafluorophenol (1.22 g, 6.60 mmol) in CH₂Cl₂ (25 mL) at 0 °C. The reaction mixture was allowed to warm to room temperature and stirred for 16 h. The resultant homogenous solution was diluted with CH₂Cl₂ (20 mL) and washed

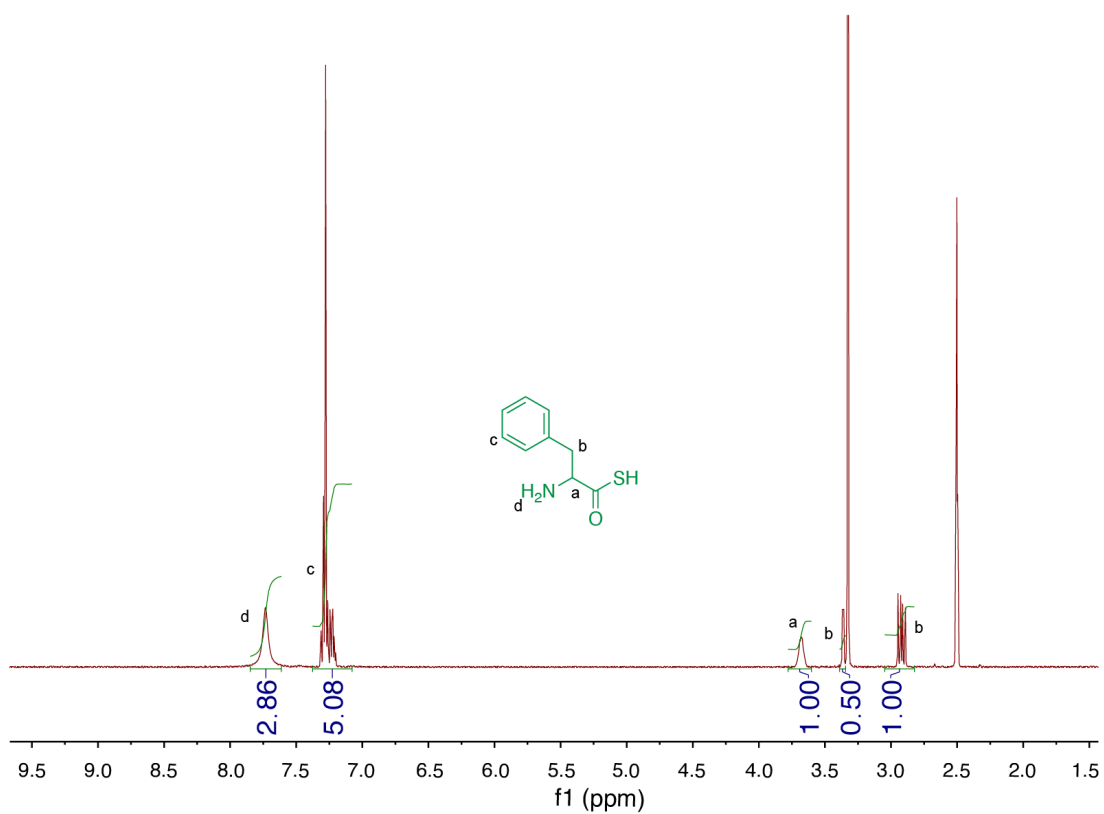
with water (2 x 20 mL), NaHCO₃ (sat., 2 x 20 mL) and brine (20 mL). The organic layer was dried over Na₂SO₄, filtered, and concentrated in vacuo to give *N*-acetylglycine pentafluorophenyl ester **Ac-Gly-OPfp**, which was used immediately without further purification. The crude **Ac-Gly-OPfp** was resuspended in anhydrous acetonitrile (15 mL) and stirred vigorously with anhydrous sodium sulfide (1.1 equiv) under argon atmosphere for 6 h at room temperature. The resultant precipitate was isolated by centrifugation and washed with diethyl ether (3× 10mL) and lyophilized to yield **Ac-Gly-S⁻Na⁺** as a white solid (350 mg). ¹H NMR (400 MHz, D₂O): d 4.08 (s, 2H, (C2)-H₂), 1.97 (s, 3H, (COCH₃)). HRMS-ESI [M-H]⁻ calcd. for [C₄H₇NO₂S-H]⁻: 132.0119; observed: 132.0117.



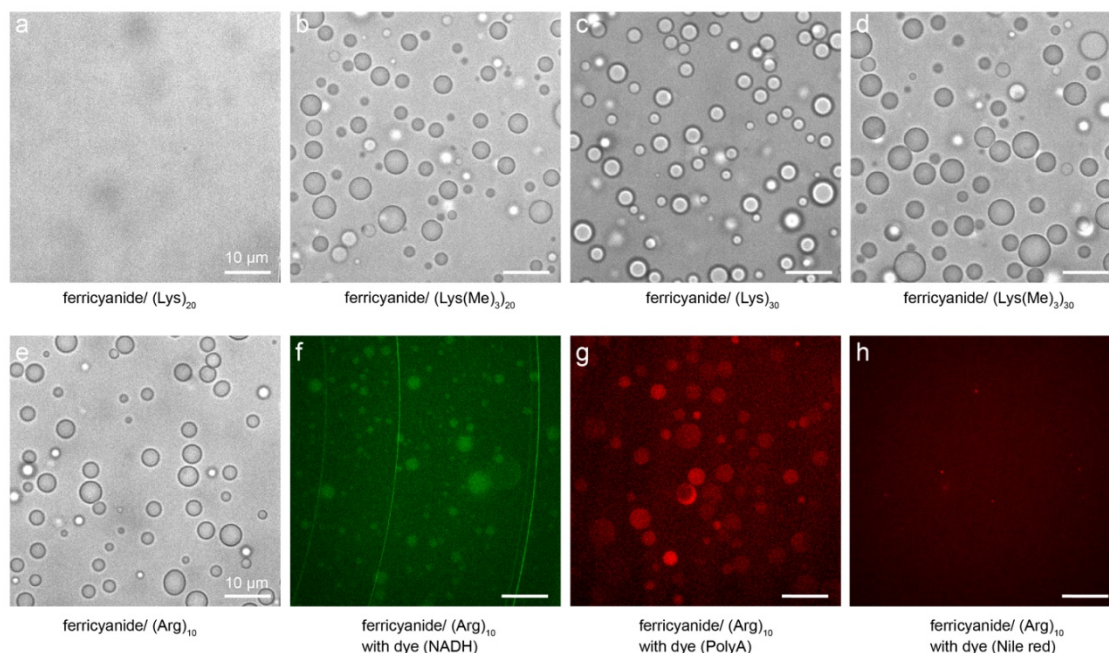
Supplementary Figure 1. ¹H-NMR spectrum of Ac-Gly-S⁻Na⁺ (400 MHz, D₂O).



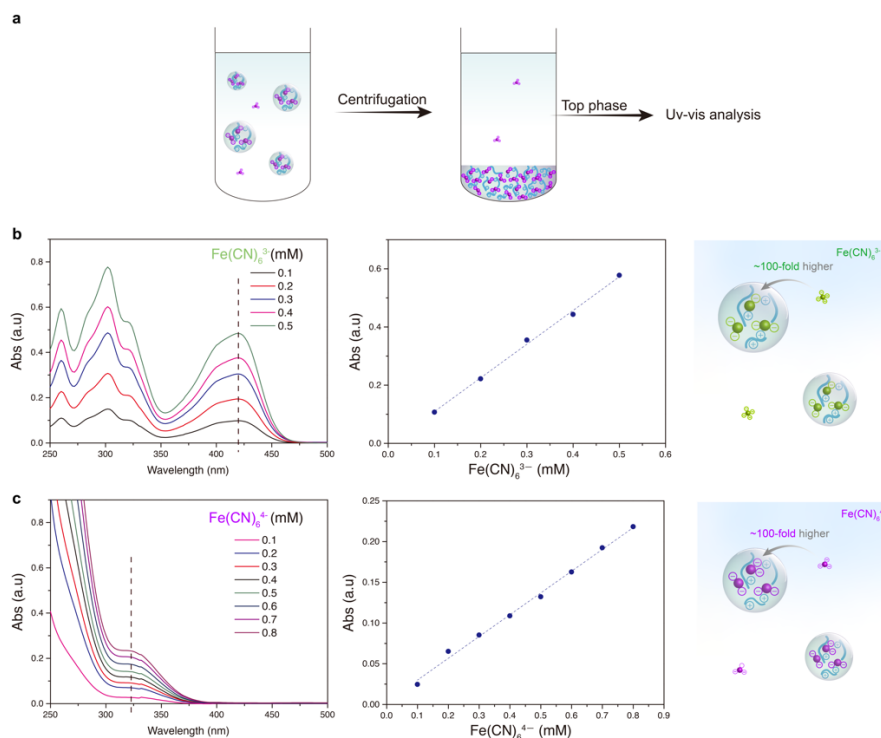
Supplementary Figure 2. ¹H-NMR spectrum of Ac-Phe-S-Na⁺ (400 MHz, D₂O)



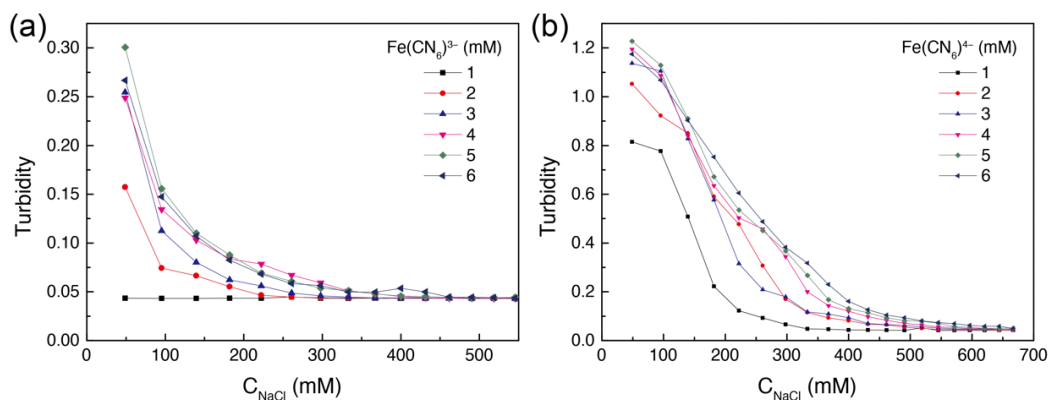
Supplementary Figure 3. ¹H-NMR spectrum of Phe-SH (400 MHz, DMSO-D₆).



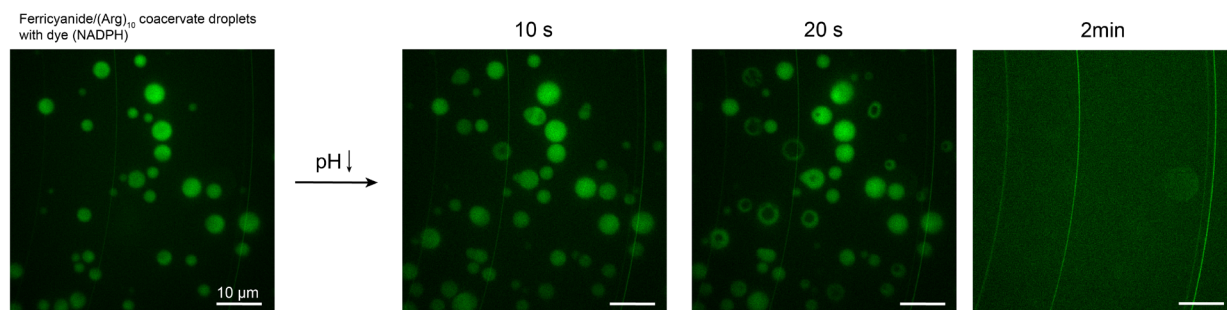
Supplementary Figure 4. Optical microscope images of ferricyanide/(Lys)₂₀ (a), ferricyanide/(Lys(Me)₃)₂₀ (b), ferricyanide/(Lys)₃₀ (c), ferricyanide/(Lys(Me)₃)₃₀ (d), and ferricyanide/(Arg)₁₀ (e) coacervates. Fluorescence images of ferricyanide/(Arg)₁₀ coacervate droplets selectively uptake of NADH (f), Poly-A₁₅ (Cy5-A₁₅) (g), and Nile red (h).



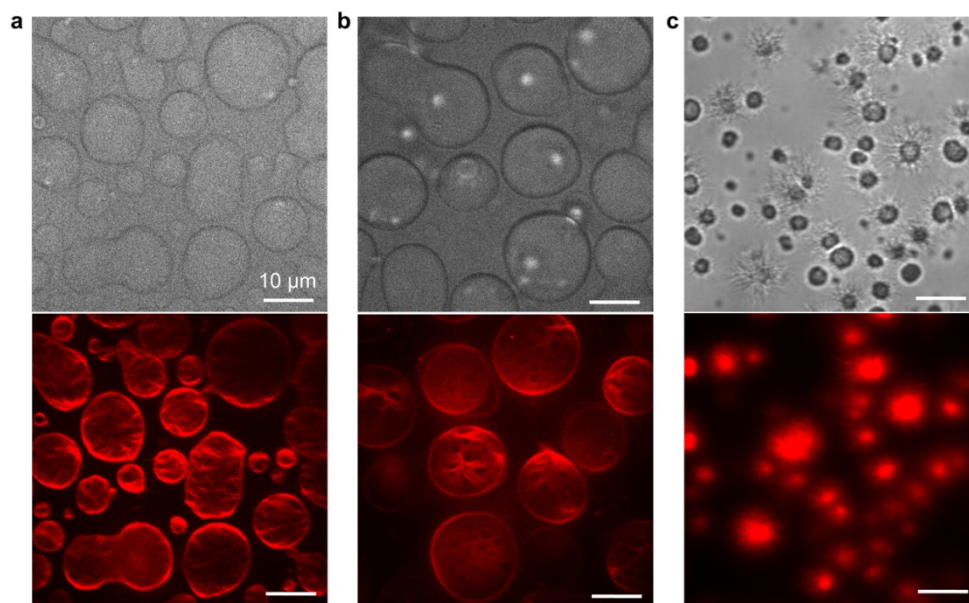
Supplementary Figure 5. (a) Scheme of the method to determine the ferricyanide concentrations inside and outside the droplet phase. (b, c) UV-vis spectra of the ferricyanide or ferrocyanide concentration in top phase at different concentrations, and the corresponding standard curve of the ferricyanide/ferrocyanide absorbance. We calculated the ferricyanide and ferrocyanide concentrations of the top solution from the standard curve, and then the ferricyanide and ferrocyanide concentrations inside the coacervate phase can be known.



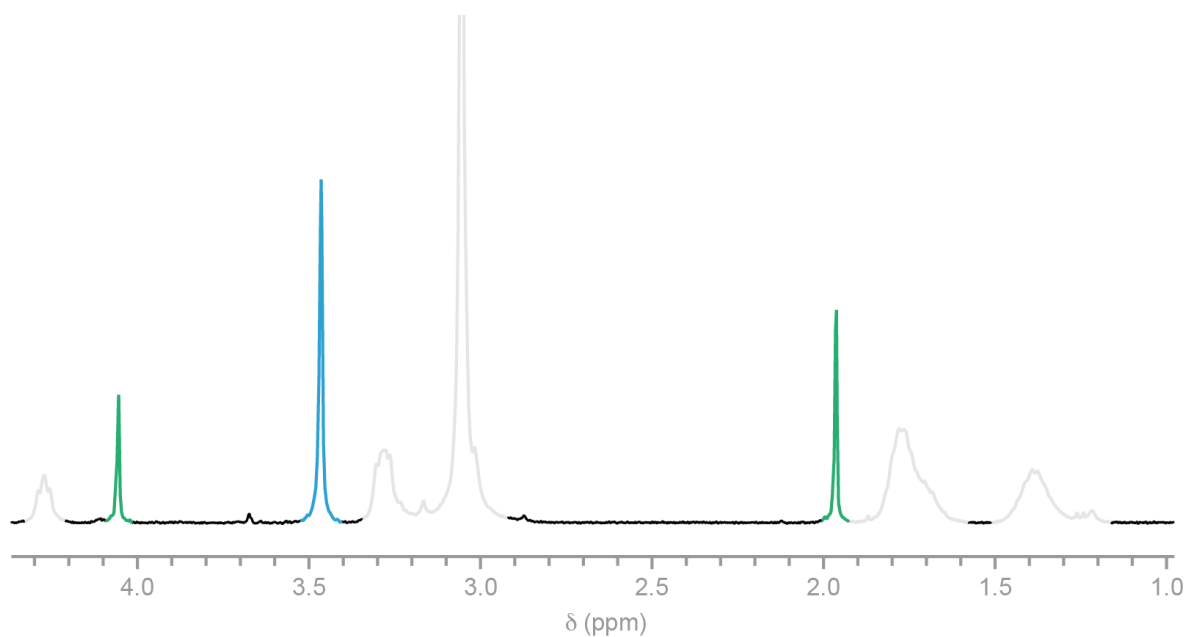
Supplementary Figure 6. Turbidity of $\text{Fe}(\text{CN})_6^{3-}/\text{Fe}(\text{CN})_6^{4-}$ -pLys mixtures as a function of concentration of added NaCl (a and b). The mixtures contained a fixed concentration of 50 mM Tris buffer, 5 mM pLys (monomer units). The mixtures containing ferricyanide were titrated with NaCl 0.5 M, while the mixtures containing Ferrocyanide were titrated with NaCl 2 M.



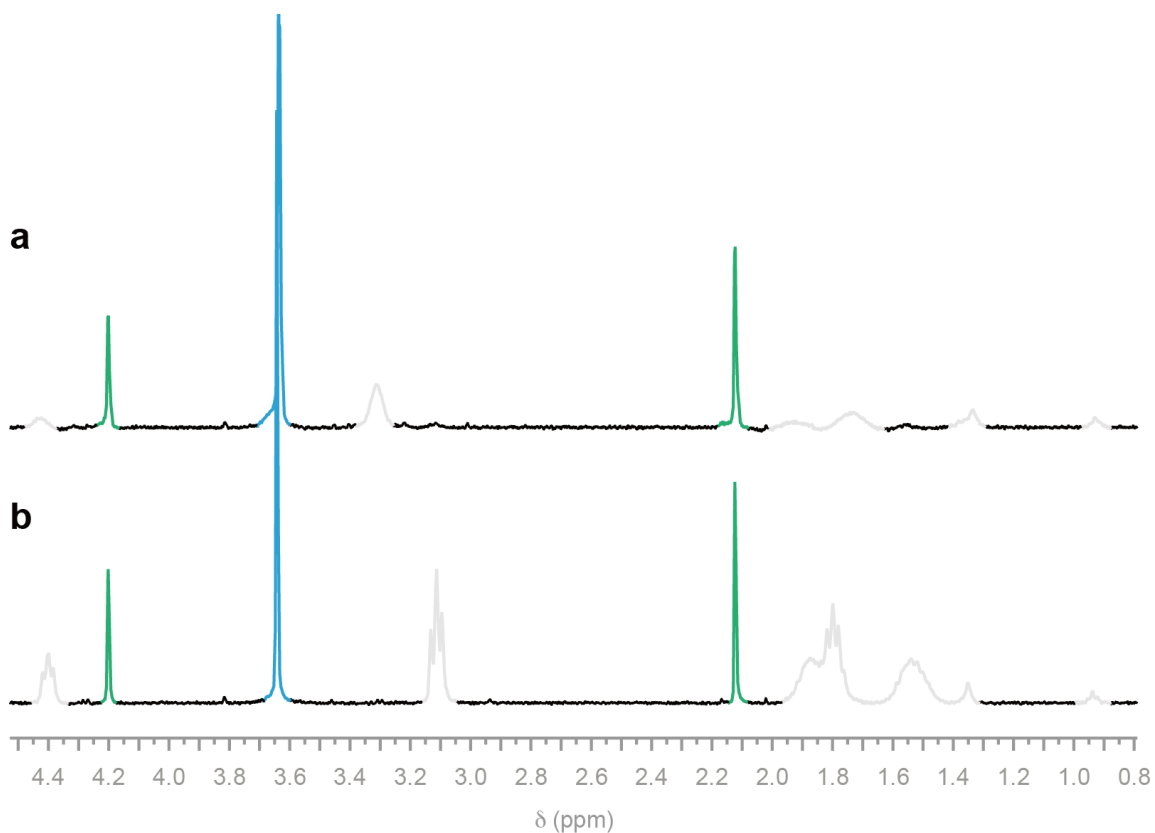
Supplementary Figure 7. Confocal micrographs of ferricyanide/(Arg)₁₀ protocells (stained with NADH), time series of representative protocells after pH-triggered redox reaction.



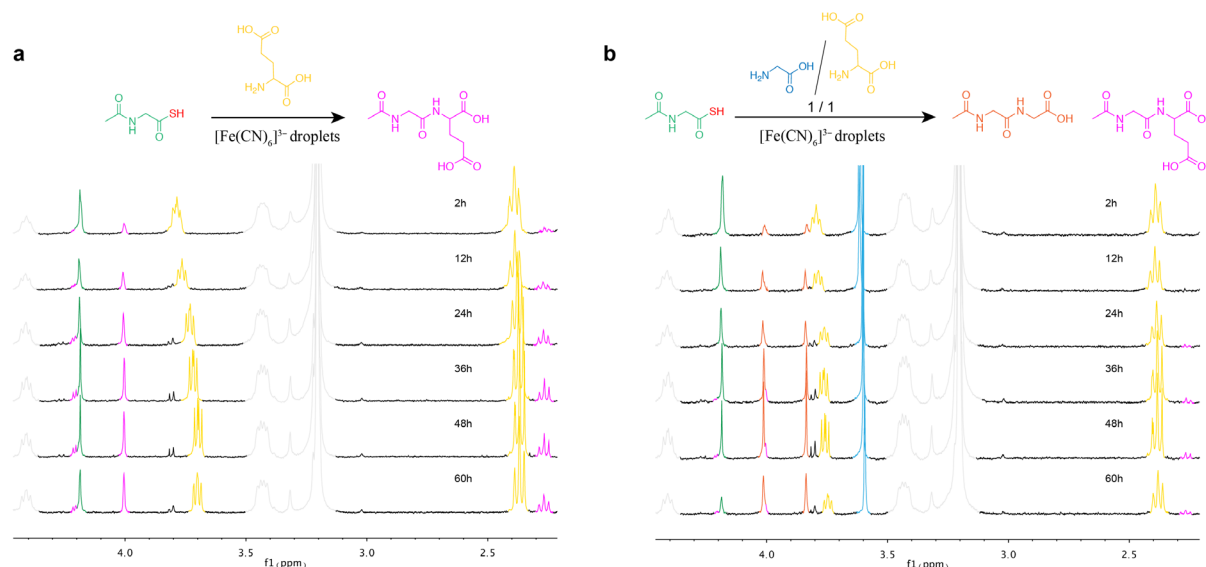
Supplementary Figure 8. Confocal micrographs of ferricyanide/(Lys(Me)₃)₂₀ (a), ferricyanide/(Lys(Me)₃)₃₀ (b), and ferricyanide/(Lys)₃₀ (c) protocells (with dye, Nile red) after addition of BC. Scale bar, 10 μm .



Supplementary Figure 9. ^1H NMR spectrum of peptide ligation reaction in control solution without ferricyanide, no ligation product observed after 3 h. (Ac-Gly-SH (8mM, green), Gly (3 equiv., blue), (ferrocyanide, 6mM), ((Lys(Me)₃)₃₀, gray)).



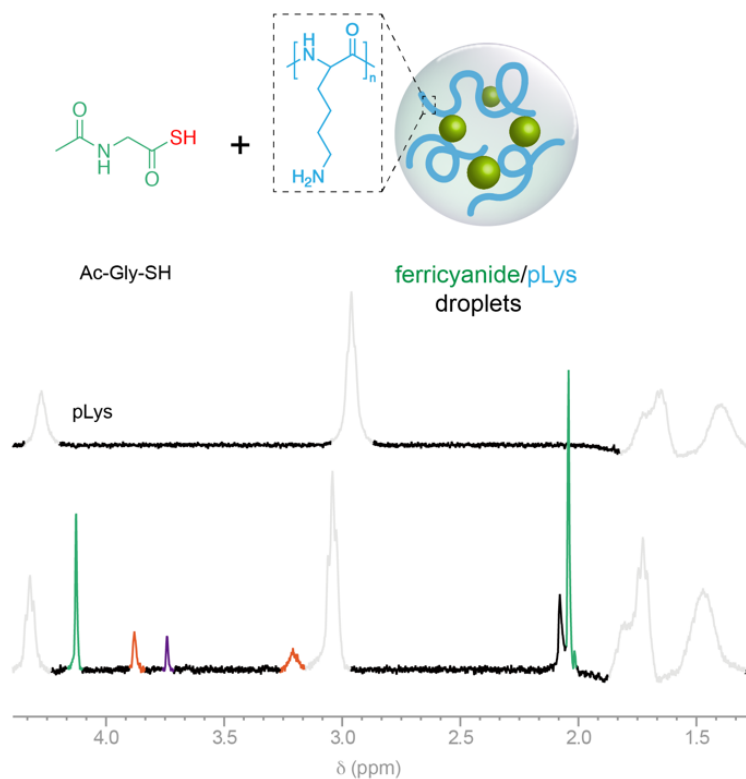
Supplementary Figure 10. ^1H NMR spectrum of peptide ligation reaction in ferrocyanide/(Arg)₁₀ (a) and ferrocyanide/(Lys)₂₀ protocells, no ligation product observed after 3 h. (Ac-Gly-SH (8mM, green), Gly (3 equiv., blue), (ferrocyanide, 6mM), (polycations, gray)).



Supplementary Figure 11. (a) Time series of ^1H NMR spectrum of peptide ligation reaction in ferricyanide/ $(\text{Lys}(\text{Me})_3)_{20}$ protocells. (Ac-Gly-SH (8 mM, green), Glu (24 mM, yellow), (ferricyanide, 8 mM), (polycations, gray)). (b) Time series of ^1H NMR spectrum of peptide ligation reaction in ferricyanide/ $(\text{Lys}(\text{Me})_3)_{20}$ protocells. (Ac-Gly-SH (8 mM, green), Glu (12 mM, yellow), Gly (12 mM, blue) (ferricyanide, 8mM), (polycations, gray)).

Supplementary Table 1. Yields for the products of prebiotic oxidative coupling of α -aminoacetyl thioacid Ac-Gly-SH (8 mM) with amino acid mixture AA_1/AA_2 (ratio 1:1, 12 mM: 12 mM) and Ferricyanide (8 mM)/ $(\text{Lys}(\text{Me})_3)_{20}$ (Lys monomer 24 mM) coacervates dispersion, pH 9, unless stated otherwise.

Amino Acid mixture $\text{AA}_1:\text{AA}_2$ 1:1	Yield ratio Ac-Gly- AA_1 -OH(%) : Ac-Gly- AA_2 -OH(%)	
	Time (h)	
	4 h	60 h
Gly:Glu	10:0	10:1
Gly:Ala	6:1	5:1
Gly:Phe	4.8:1	3.5:1
Ala:Glu	1.7:1	1.5:1
Glu:Phe	3.5:1	1.7:1



Supplementary Figure 12. ^1H NMR spectrum showing the thioacid ligation reaction of Ac-Gly-SH (8 mM, green) with ferricyanide (8 mM)/pLys (15-30K, Lys monomer 24 mM, gray) coacervates to yield pLys ϵ -NH₂ ligation (orange).

Supplementary references

1. Okamoto, R.; Haraguchi, T.; Nomura, K.; Maki, Y.; Izumi, M.; Kajihara, Y., Regioselective alpha-Peptide Bond Formation Through the Oxidation of Amino Thioacids. *Biochemistry* **2019**, *58* (12), 1672-1678.
2. Canavelli, P.; Islam, S.; Powner, M. W., Peptide ligation by chemoselective aminonitrile coupling in water. *Nature* **2019**, *571* (7766), 546-549.
3. Granados, E. N.; Bello, J., Alkylated poly(amino acids). I. Conformational properties of poly(N ϵ -trimethyl- L-lysine) and poly(N δ -trimethyl-L-ornithine). *Biopolymers* **1976**, *18*, 1479-1486.